Communications in Physics, Vol. 33, No. 3 (2023), pp. 223-234
DOI: https://doi.org/10.15625/0868-3166/18077

Enhancing the doubly-longitudinal polarization in WZ production at the LHC

Thi Nhung Dao and Duc Ninh Le[†]

Faculty of Fundamental Sciences, PHENIKAA University, Hanoi 12116, Vietnam

E-mail: [†]ninh.leduc@phenikaa-uni.edu.vn

Received 17 February 2023
Accepted for publication 12 May 2023
Published 30 June 2023

Abstract. *We present new results for the theoretical prediction of doubly-polarized cross sections of WZ events at the LHC using leptonic decays. Compared to the previous studies, two new kinematic cuts are considered. These cuts are designed to enhance the doubly-longitudinal (LL) polarization and, at the same time, study the Radiation Amplitude Zero effect. We found a new cut on the rapidity separation between the Z boson and the electron from the W decay which makes the LL fraction largest, namely $|\Delta y_{Z,e}| < 0.5$. This result is obtained at the next-to-leading order in the strong and electroweak couplings.*

Keywords: Collider physics, diboson, electroweak interactions, polarization.
Classification numbers: 12.15.-y, 14.70.Fm, 14.70.Hp.

1. Introduction

With the new results from ATLAS [1], where doubly-polarized cross sections of the diboson $W^{\pm}Z$ production at the Large Hadron Collider (LHC) are measured for the first time using the Run-2 data set and that the LHC Run 3 already began in July 2022, there is a foundation to expect that more precise measurements of diboson joint-polarization cross sections from ATLAS and CMS will come soon.

Measuring the doubly-polarized cross sections in diboson production processes allows for testing the Standard Model (SM) at a deeper level. This is because the longitudinal component of a massive gauge boson comes from the spontaneous symmetry breaking mechanism (SSB). Studying the longitudinally polarized cross sections, in particular the doubly longitudinal one, therefore gives us valuable information about the SSB mechanism. Moreover, polarization observables such as kinematic distributions of polarized events, polarization fractions or angular coefficients

can provide better discrimination power to identify new physics, e.g. to determine the spin of the intermediate particles decaying into two gauge bosons (see e.g. Ref. [2] for the differences between spin-0 and spin-1 cases).

Recent theoretical works to define the signal part of the doubly-polarized cross sections using the double-pole approximation (DPA) were able to provide results at the next-to-leading-order (NLO) in QCD for W^+W^- [3], WZ [4–7], ZZ [8] and at NLO in the electroweak (EW) interactions for ZZ [8] and WZ [5, 6]. For the case of W^+W^-, the next-to-next-to-leading-order QCD results are available [9].

In our previous works [5, 6] the momenta of the final-state leptons are selected according to the ATLAS fiducial phase-space cut (named Cut 1 in this paper) as defined in Refs. [1, 10, 11]. After discussions with experimental colleagues, we realized that other phase-space cuts (Cut 2 and Cut 3 in this paper) should be explored as well. These new kinematic setups are designed to enhance the doubly longitudinal (LL) polarization [12] and observe the Radiation Amplitude Zero (RAZ) effect [13]. The purpose of this work is to explore these setups in the hope of finding optimal features for the study of the LL polarization in WZ events.

The paper is organized as follows. We first define the polarized cross sections in Sec. 2, before presenting the numerical results in Sec. 3. Conclusions are provided in Sec. 4.

2. Definition of polarized cross sections

In order to set up our notations, we briefly review here the definition of the polarized cross sections. We use the same conventions and calculation setup as in [6]. The process of interest, which is measured at the LHC, reads

$$p(k_1) + p(k_2) \to \ell_1(k_3) + \ell_2(k_4) + \ell_3(k_5) + \ell_4(k_6) + X, \tag{1}$$

where the final-state leptons can be either $e^+\nu_e\mu^+\mu^-$ or $e^-\bar{\nu}_e\mu^+\mu^-$. Representative Feynman diagrams at leading order (LO) are depicted in Fig. 1.

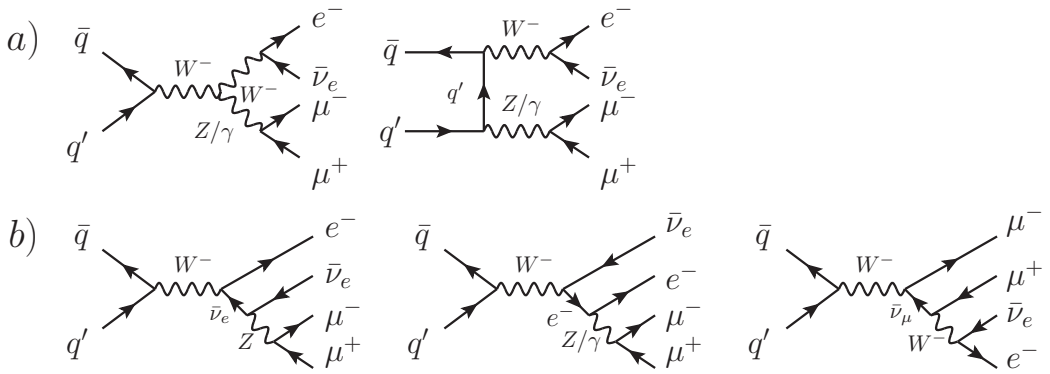

Fig. 1. Double and single resonant diagrams at leading order. Group a) includes both double (WZ) and single ($W\gamma$) resonant diagrams, while group b) is only single resonant.

From Fig. 1 we see that the doubly-polarized WZ events, which occur via the double-resonant WZ diagrams in the group a), are mixed with the single resonant events. Theoretically, we cannot just select those WZ double resonant diagrams because they are linked with the single

resonant diagrams by gauge invariance. To separate the WZ events we need to use a special technique called the double-pole approximation, which selects only the gauge-invariance part of the WZ double resonant cross section. We note that the DPA has been widely used in diboson production processes, see Ref. [14] and references therein.

To be more concrete, the WZ double resonant processes are written as

$$p(k_1)+p(k_2)\to V_1(q_1)+V_2(q_2)\to \ell_1(k_3)+\ell_2(k_4)+\ell_3(k_5)+\ell_4(k_6)+X, \tag{2}$$

where the intermediate gauge bosons are $V_1=W^{\pm}$, $V_2=Z$. Hence the double-pole unpolarized amplitude at leading order (LO) can be expressed as

$$\mathscr{A}^{\bar{q}q'\to V_1V_2\to 4l}_{\rm LO,DPA}=\frac{1}{Q_1Q_2}\sum_{\lambda_1,\lambda_2=1}^{3}\mathscr{A}^{\bar{q}q'\to V_1V_2}_{\rm LO}(\hat{k}_i)\mathscr{A}^{V_1\to\ell_1\ell_2}_{\rm LO}(\hat{k}_i)\mathscr{A}^{V_2\to\ell_3\ell_4}_{\rm LO}(\hat{k}_i), \tag{3}$$

with

$$Q_j=q_j^2-M_{V_j}^2+iM_{V_j}\Gamma_{V_j}\,(j=1,2), \tag{4}$$

where $q_1=k_3+k_4$, $q_2=k_5+k_6$, M_V and Γ_V are the physical mass and width of the gauge boson V, and λ_j are the polarization indices of the gauge bosons. Note that the helicity indices of the initial quarks and final leptons are implicit. It is crucial that all helicity amplitudes $\mathscr{A}$ in the r.h.s. are calculated using on-shell (OS) momenta $\hat{k}_i$ for the final-state leptons as well as OS momenta $\hat{q}_j$ for the intermediate gauge bosons, derived from the off-shell (full process) momenta k_i and q_j, in order to ensure that gauge invariance in the amplitudes is preserved. An OS mapping is used to obtain the OS momenta $\hat{k}_i$ from the off-shell momenta k_i. This OS mapping is not unique, however the shift induced by different mappings is of order $\alpha\Gamma_V/(\pi M_V)$ [14]. The OS mapping used in this paper is the same as in Ref. [6].

Eq. (3) serves as the master equation to define the doubly polarized cross sections. Since a massive gauge boson has three physical polarization states: two transverse states $\lambda=1$ and $\lambda=3$ (left and right) and one longitudinal state $\lambda=2$, the WZ system has in total 9 polarization states. The unpolarized amplitude defined in Eq. (3) is the sum of these 9 polarized amplitudes. The unpolarized cross section is then divided into the following five terms:

- W_LZ_L: The longitudinal-longitudinal (LL) contribution, obtained with selecting $\lambda_1=\lambda_2=2$ in the sum of Eq. (3);
- W_LZ_T: The longitudinal-transverse (LT) contribution, obtained with selecting $\lambda_1=2$, $\lambda_2=1,3$. The LT cross section includes the interference term between the (21) and (23) amplitudes.
- W_TZ_L: The transverse-longitudinal (TL) contribution, obtained with selecting $\lambda_1=1,3$, $\lambda_2=2$. The interference between the (12) and (32) amplitudes is here included.
- W_TZ_T: The transverse-transverse (TT) contribution, obtained with selecting $\lambda_1=1,3$, $\lambda_2=1,3$. The interference terms between the (11), (13), (31), (33) amplitudes are here included.
- Interference: This includes the interference terms between the above LL, LT, TL, TT amplitudes.

Our doubly-polarized cross-section results include not only the leading order but also the NLO QCD and EW corrections. The expressions for double-pole unpolarized amplitudes need to be extended to include also the virtual corrections, the gluon/photon induced and radiation processes

as done in Ref. [6]. In this short writing the above LO definition of the polarized cross sections is enough for the reader to understand the numerical results discussed in the next section.

3. Numerical results

Our numerical results are obtained for proton-proton collisions at a center-of-mass energy of 13 TeV. Fixed factorization and renormalization scales are used, namely $\mu_F = \mu_R = \mu_0 = (M_W + M_Z)/2$, where $M_W = 80.385\,\text{GeV}$ and $M_Z = 91.1876\,\text{GeV}$. For the parton distribution functions (PDF) and value of the strong coupling constant, the Hessian set `LUXqed17_plus_PDF4LHC15_nnlo_30` [15–24] via the library `LHAPDF6` [25] is employed. More details about other input parameters are provided in Ref. [6].

For NLO EW corrections, an additional photon can be emitted. Hence, the lepton-photon recombination to define a dressed lepton is done before applying the analysis cuts. A dressed lepton has the momentum of $p'_\ell = p_\ell + p_\gamma$ if the angular distance $\Delta R(\ell,\gamma) \equiv \sqrt{(\Delta\eta)^2 + (\Delta\phi)^2} < 0.1$, i.e. when the photon is close enough to the bare lepton. Here the letter ℓ denotes e or μ and all momenta are calculated in the Lab frame. All leptons and quarks except for the top quark are approximated as massless.

The doubly polarized cross sections and distributions depend on the reference frame. We choose the WZ center-of-mass frame, the same as in the ATLAS measurement [1]. We now specify the three cut setups used in this paper. They read as follows.

3.0.0.1. Cut 1: The baseline setup, called Cut 1, is the ATLAS fiducial set of cuts used in Refs. [1, 10, 11], which reads

$$\begin{aligned} p_{T,e} > 20\,\text{GeV}, \quad p_{T,\mu^\pm} > 15\,\text{GeV}, \quad |\eta_\ell| < 2.5, \\ \Delta R\left(\mu^+,\mu^-\right) > 0.2, \quad \Delta R\left(e,\mu^\pm\right) > 0.3, \\ m_{T,W} > 30\,\text{GeV}, \quad \left|m_{\mu^+\mu^-} - M_Z\right| < 10\,\text{GeV}, \end{aligned} \tag{5}$$

where $m_{T,W} = \sqrt{2 p_{T,\nu} p_{T,e} [1 - \cos\Delta\phi(e,\nu)]}$ with $\Delta\phi(e,\nu)$ being the angle between the electron and the neutrino in the transverse plane. This Cut 1 was used in our previous studies [5, 6].

3.0.0.2. Cut 2: In addition to the cuts in Cut 1, we further require that the transverse momentum of the WZ system satisfies [12]

$$p_{T,WZ} < 70\,\text{GeV}. \tag{6}$$

At NLO, this additional cut affects only the real-emission contributions with an extra particle in the final state. The LO term and virtual corrections are unaffected. The purpose of this cut is to observe the RAZ in the TT component, which is smeared out by QCD radiation [12, 13]. This cut reduces higher-order QCD corrections. Dominant backgrounds, in particular $t\bar{t}$, $t\bar{t}V$, VVV are expected to decrease significantly by this cut as well.

3.0.0.3. Cut 3: In addition to the cuts in Cut 2, we further require [12]

$$p_{T,Z} > 200\,\text{GeV}. \tag{7}$$

This additional cut reduces drastically the LO contribution as well as all NLO corrections. The purpose of this cut is to focus more on the high energy regime where new physics effects are expected to be present. As will be seen, this cut will increase the LL fraction significantly.

Table 1. Unpolarized (Unpol.) and doubly polarized cross sections in fb together with polarization fractions calculated at LO, NLO EW, NLO QCD, and NLO QCD+EW, all in the DPA, in the WZ center-of-mass system for the W^+Z process. The interference (Inter.) between the polarized amplitudes is provided in the bottom row. The statistical uncertainties (in parenthesis) are given on the last digits of the central prediction when significant. Seven-point scale uncertainty is also provided for the cross sections as sub- and superscripts in percent. In the last column the EW correction relative to the NLO QCD prediction is given.

	$\sigma_{\rm LO}$ [fb]	$f_{\rm LO}$ [%]	$\sigma^{\rm EW}_{\rm NLO}$ [fb]	$f^{\rm EW}_{\rm NLO}$ [%]	$\sigma^{\rm QCD}_{\rm NLO}$ [fb]	$f^{\rm QCD}_{\rm NLO}$ [%]	$\sigma^{\rm QCDEW}_{\rm NLO}$ [fb]	$f^{\rm QCDEW}_{\rm NLO}$ [%]	$\bar{\delta}_{\rm EW}$ [%]
Unpol., Cut 1	$18.934(1)^{+4.8\%}_{-5.9\%}$	100	$18.138(1)^{+4.9\%}_{-6.0\%}$	100	$34.071(2)^{+5.3\%}_{-4.2\%}$	100	$33.275(2)^{+5.4\%}_{-4.3\%}$	100	−2.3
Cut 2	$18.934(1)^{+4.8\%}_{-5.9\%}$	100	$17.897(1)^{+4.9\%}_{-6.0\%}$	100	$25.860(3)^{+3.2\%}_{-2.5\%}$	100	$24.823(3)^{+3.4\%}_{-2.6\%}$	100	−4.0
Cut 3	$0.392^{+1.4\%}_{-1.8\%}$	100	$0.343^{+1.1\%}_{-1.5\%}$	100	$0.445^{+2.2\%}_{-1.5\%}$	100	$0.396^{+2.0\%}_{-1.2\%}$	100	−11.0
$W^+_L Z_L$, Cut 1	$1.492^{+5.1\%}_{-6.3\%}$	7.9	$1.428^{+5.2\%}_{-6.4\%}$	7.9	$1.938^{+2.7\%}_{-2.2\%}$	5.7	$1.874^{+2.8\%}_{-2.3\%}$	5.6	−3.3
Cut 2	$1.492^{+5.1\%}_{-6.3\%}$	7.9	$1.420^{+5.3\%}_{-6.4\%}$	7.9	$1.786^{+1.9\%}_{-2.3\%}$	6.9	$1.714^{+2.0\%}_{-2.2\%}$	6.9	−4.0
Cut 3	$0.105^{+0.0\%}_{-0.7\%}$	26.7	$0.092^{+0.0\%}_{-0.5\%}$	26.9	$0.100^{+0.8\%}_{-0.6\%}$	22.6	$0.088^{+1.2\%}_{-1.0\%}$	22.2	−13.0
$W^+_L Z_T$, Cut 1	$2.018^{+5.8\%}_{-7.0\%}$	10.7	$1.951^{+5.8\%}_{-7.0\%}$	10.8	$5.273^{+7.3\%}_{-5.9\%}$	15.5	$5.207^{+7.4\%}_{-6.0\%}$	15.6	−1.3
Cut 2	$2.018^{+5.8\%}_{-7.0\%}$	10.7	$1.928^{+5.8\%}_{-7.0\%}$	10.8	$3.419^{+4.9\%}_{-3.8\%}$	13.2	$3.329^{+5.1\%}_{-3.9\%}$	13.4	−2.6
Cut 3	$0.017^{+0.0\%}_{-0.4\%}$	4.4	$0.016^{+0.0\%}_{-0.5\%}$	4.8	$0.023^{+3.9\%}_{-2.9\%}$	5.1	$0.022^{+3.9\%}_{-2.9\%}$	5.5	−4.3
$W^+_T Z_L$, Cut 1	$1.903^{+5.7\%}_{-6.9\%}$	10.1	$1.893^{+5.7\%}_{-6.9\%}$	10.4	$5.024^{+7.4\%}_{-5.9\%}$	14.7	$5.013^{+7.4\%}_{-5.9\%}$	15.1	−0.2
Cut 2	$1.903^{+5.7\%}_{-6.9\%}$	10.1	$1.826^{+5.8\%}_{-7.0\%}$	10.2	$3.281^{+5.0\%}_{-4.0\%}$	12.7	$3.204^{+5.1\%}_{-4.1\%}$	12.9	−2.3
Cut 3	$0.017^{+0.0\%}_{-0.4\%}$	4.3	$0.017^{+0.0\%}_{-0.5\%}$	4.9	$0.021^{+3.1\%}_{-2.5\%}$	4.6	$0.020^{+3.0\%}_{-2.3\%}$	5.2	0.0
$W^+_T Z_T$, Cut 1	$13.376^{+4.5\%}_{-5.6\%}$	70.6	$12.728(1)^{+4.6\%}_{-5.7\%}$	70.2	$21.626(2)^{+4.5\%}_{-3.6\%}$	63.5	$20.977(2)^{+4.7\%}_{-3.8\%}$	63.0	−3.0
Cut 2	$13.376^{+4.5\%}_{-5.6\%}$	70.6	$12.587(1)^{+4.5\%}_{-5.7\%}$	70.3	$17.132(2)^{+2.6\%}_{-2.1\%}$	66.2	$16.342(2)^{+2.7\%}_{-2.2\%}$	65.8	−4.6
Cut 3	$0.247^{+2.2\%}_{-2.5\%}$	63.1	$0.212^{+1.9\%}_{-2.1\%}$	61.9	$0.297^{+3.1\%}_{-2.1\%}$	66.7	$0.262^{+3.0\%}_{-1.7\%}$	66.1	−11.8
Inter., Cut 1	0.144(1)	0.8	0.138(1)	0.8	0.210(3)	0.6	0.204(3)	0.6	−2.9
Cut 2	0.144(1)	0.8	0.137(1)	0.8	0.242(3)	0.9	0.235(3)	0.9	−2.9
Cut 3	0.006	1.5	0.005	1.6	0.005	1.0	0.004	1.0	−20.0

3.1. Integrated polarized cross sections

We first present results for the integrated cross sections at LO, NLO QCD, NLO EW, and NLO QCD+EW for the unpolarized case, LL, LT, TL, TT polarizations and the interference in Table 1 for the case of W^+Z and in Table 2 for W^-Z for all three cut setups. The results for Cut 1 have already been published in Refs. [5,6]. They are re-provided here for the sake of comparison.

Included in the two tables are also the polarization fractions, f, calculated as ratios of the polarized cross sections over the unpolarized cross section at each level of accuracy. The total EW correction relative to the NLO QCD prediction is defined as

$$\bar{\delta}_{\rm EW} = (\sigma^{\rm EW}_{\rm NLO} - \sigma_{\rm LO})/\sigma^{\rm QCD}_{\rm NLO}. \tag{8}$$

Table 2. Same as Table 1 but for the W^-Z process.

	$\sigma_{\rm LO}$ [fb]	$f_{\rm LO}$ [%]	$\sigma^{\rm EW}_{\rm NLO}$ [fb]	$f^{\rm EW}_{\rm NLO}$ [%]	$\sigma^{\rm QCD}_{\rm NLO}$ [fb]	$f^{\rm QCD}_{\rm NLO}$ [%]	$\sigma^{\rm QCDEW}_{\rm NLO}$ [fb]	$f^{\rm QCDEW}_{\rm NLO}$ [%]	$\tilde{\delta}_{\rm EW}$ [%]
Unpol., Cut 1	$12.745^{+4.9\%}_{-6.2\%}$	100	$12.224^{+5.1\%}_{-6.3\%}$	100	$23.705(1)^{+5.5\%}_{-4.4\%}$	100	$23.184(1)^{+5.6\%}_{-4.5\%}$	100	-2.2
Cut 2	$12.745^{+4.9\%}_{-6.2\%}$	100	$12.060(1)^{+5.1\%}_{-6.3\%}$	100	$17.905(2)^{+3.4\%}_{-2.7\%}$	100	$17.221(2)^{+3.5\%}_{-2.8\%}$	100	-3.8
Cut 3	$0.209^{+1.3\%}_{-1.8\%}$	100	$0.184^{+1.0\%}_{-1.5\%}$	100	$0.259^{+3.3\%}_{-2.7\%}$	100	$0.234^{+3.2\%}_{-2.5\%}$	100	-9.7
$W_L^-Z_L$, Cut 1	$1.094^{+5.2\%}_{-6.5\%}$	8.6	$1.048^{+5.3\%}_{-6.6\%}$	8.6	$1.407^{+2.6\%}_{-2.1\%}$	5.9	$1.361^{+2.7\%}_{-2.2\%}$	5.9	-3.3
Cut 2	$1.094^{+5.2\%}_{-6.5\%}$	8.6	$1.043^{+5.3\%}_{-6.6\%}$	8.6	$1.308^{+1.9\%}_{-2.3\%}$	7.3	$1.257^{+2.0\%}_{-2.3\%}$	7.3	-3.9
Cut 3	$0.059^{+0.1\%}_{-0.8\%}$	28.4	$0.052^{+0.0\%}_{-0.6\%}$	28.5	$0.057^{+0.7\%}_{-0.4\%}$	22.2	$0.051^{+1.1\%}_{-0.7\%}$	21.6	-12.3
$W_L^-Z_T$, Cut 1	$1.508^{+5.8\%}_{-7.0\%}$	11.8	$1.456^{+5.9\%}_{-7.1\%}$	11.9	$3.921^{+7.3\%}_{-5.9\%}$	16.5	$3.869^{+7.4\%}_{-6.0\%}$	16.7	-1.3
Cut 2	$1.508^{+5.8\%}_{-7.0\%}$	11.8	$1.440^{+5.8\%}_{-7.1\%}$	11.9	$2.605^{+5.0\%}_{-4.0\%}$	14.5	$2.536^{+5.2\%}_{-4.1\%}$	14.7	-2.6
Cut 3	$0.010^{+0.0}_{-0.5\%}$	4.8	$0.010^{+0.0\%}_{-0.4\%}$	5.2	$0.015^{+5.3\%}_{-4.2\%}$	5.8	$0.014^{+5.4\%}_{-4.2\%}$	6.2	0.0
$W_T^-Z_L$, Cut 1	$1.356^{+5.8\%}_{-7.0\%}$	10.6	$1.347^{+5.8\%}_{-7.0\%}$	11.0	$3.606^{+7.4\%}_{-6.0\%}$	15.2	$3.597^{+7.4\%}_{-6.0\%}$	15.5	-0.2
Cut 2	$1.356^{+5.8\%}_{-7.0\%}$	10.6	$1.302^{+5.9\%}_{-7.1\%}$	10.8	$2.375^{+5.1\%}_{-4.1\%}$	13.3	$2.322^{+5.2\%}_{-4.2\%}$	13.5	-2.3
Cut 3	$0.010^{+0.0}_{-0.5\%}$	4.7	$0.010^{+0.0\%}_{-0.4\%}$	5.2	$0.012^{+3.9\%}_{-2.5\%}$	4.7	$0.012^{+3.7\%}_{-2.3\%}$	5.1	0.0
$W_T^-Z_T$, Cut 1	$8.833^{+4.6\%}_{-5.8\%}$	69.3	$8.416^{+4.8\%}_{-5.9\%}$	68.8	$14.664(1)^{+4.7\%}_{-3.8\%}$	61.9	$14.247(1)^{+4.9\%}_{-3.9\%}$	61.5	-2.8
Cut 2	$8.833^{+4.6\%}_{-5.8\%}$	69.3	$8.321^{+4.8\%}_{-6.0\%}$	69.0	$11.549(1)^{+2.8\%}_{-2.2\%}$	64.5	$11.037(1)^{+2.9\%}_{-2.3\%}$	64.1	-4.4
Cut 3	$0.129^{2.2\%}_{-2.5\%}$	61.8	$0.111^{+1.7\%}_{-2.2\%}$	60.7	$0.174^{+4.8\%}_{-3.6\%}$	67.1	$0.156^{+4.8\%}_{-3.5\%}$	66.8	-10.3
Inter., Cut 1	$-0.046(1)$	-0.4	$-0.043(1)$	-0.4	(2)	0.5	0.110(2)	0.5	$+2.8$
Cut 2	$-0.046(1)$	-0.4	$-0.045(1)$	-0.4	0.068(2)	0.4	0.069(2)	0.4	$+1.5$
Cut 3	0.001	0.4	0.001	0.4	0.001	0.3	0.001	0.3	0.0

This information is shown in the last column. Statistical errors are very small and shown in a few places where they are significant. Scale uncertainties are much bigger and are provided for the cross sections as sub- and superscripts in percent. These uncertainties are calculated using the seven-point method where the two scales μ_F and μ_R are varied as $n\mu_0/2$ with $n = 1,2,4$ and $\mu_0 = (M_W + M_Z)/2$ being the central scale. Additional constraint $1/2 \leq \mu_R/\mu_F \leq 2$ is used to limit the number of scale choices to seven at NLO QCD. The cases $\mu_R/\mu_F = 1/4$ or 4 are excluded, being considered too extreme.

From the tables, we see that the veto cut of $p_{T,WZ} < 70$ GeV reduces the NLO QCD+EW unpolarized cross section by around 25.5% for both processes, which is almost entirely due to the reduction of the QCD correction. This reduction is however not equally distributed among different polarizations. For the W^+Z channel, they are -8.5%, -36.1, -36.1%, -22.1% for the W_LZ_L, W_LZ_T, W_TZ_L, W_TZ_T, respectively. The corresponding numbers for the W^-Z case are -7.6%, -34.5%, -35.4%, -22.5%. One notices that, for both processes, the LL component is least reduced while the mixed polarizations LT and TL are most affected by the veto cut. This is reflected in the polarization fractions. The f_{LL} is increased from 5.6% (5.9%) to 6.9% (7.3%) for the W^+Z (W^-Z) at NLO QCD+EW. Both f_{LT}, f_{TL} decrease two percent, but the doubly-tranverse polarization fraction increases from 63.0% (61.5%) to 65.8% (64.1%).

Moving to Cut 3, we see that the integrated cross sections are drastically reduced, by around 99% compared to Cut 1, for the unpolarized case and for both processes. With 139fb^{-1} data, the numbers of signal events for Cut 1 are 1190, 1900, 3100, 10900 for the LL, LT, TL, TT polarizations, summing over the two processes, as shown in Table 1 (left) of [1]. Observing that the reduction is not uniform for different polarizations, the corresponding results for Cut 3 are obtained as 51, 8, 11, 129. These numbers will increased greatly when Run-3 data is added to the analysis in the near future. The purpose of Cut 3 is to enhance the LL fraction and this can be seen clearly in the tables. The f_{LL} now reads 22.2% (21.6%) at NLO QCD+EW for W^+Z (W^-Z) process, being ranked second after the TT fraction.

Concerning the EW corrections, they are all negative (except for the interference) and their absolute values are all smaller than 5% for Cut 1 and Cut 2. For Cut 3, they are greater than 10% for the LL and TT cases, signifying the importance of the EW corrections for the future measurements of the LL fraction.

3.2. Kinematic distributions

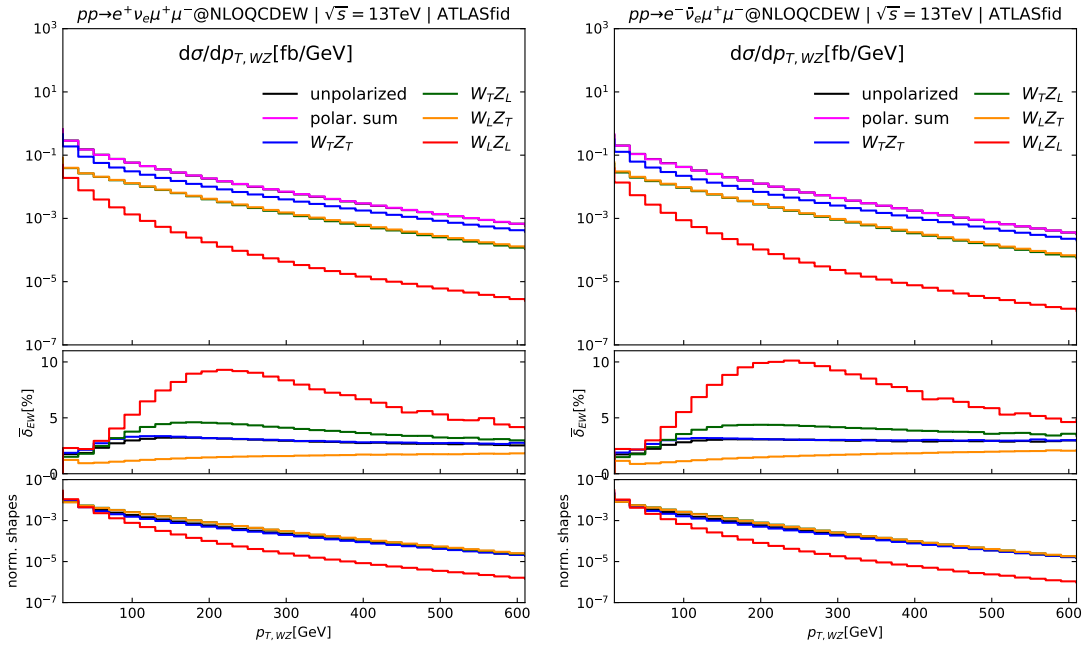

Fig. 2. Distributions in the transverse momentum of the WZ system for the W^+Z (left) and W^-Z (right) processes after Cut 1. The big panel shows the absolute values of the cross sections at NLO QCD+EW. In the bottom panel, the normalized shapes of the distributions are plotted to highlight differences in shape. The EW correction panel shows $\bar{\delta}_{\rm EW}$, the EW corrections relative to the NLO QCD cross sections, in percent (see text).

To better understand the new cuts, we show in Fig. 2 the distributions in the transverse momentum of the WZ system for the W^+Z and W^-Z processes after Cut 1. The $p_{T,Z}$ distributions have already been presented in our previous publications [5, 6]. In the big pannels, we show

the absolute values of the differential cross sections at NLO QCD+EW. In the bottom pannels, the corresponding normalized distributions (i.e. rescaling the curves so that the total area under each curve is unity) are displayed to highlight the differences in shape. In the middle pannel, the NLO EW correction with respect to the NLO QCD result, $\bar{\delta}_{\rm EW}$, is plotted. Notice that, in this special case of $p_{T,WZ}$ distribution where $p_{T,WZ} = 0$ for the LO kinematic configurations, the first contribution comes from real-emission processes at NLO for bins with $p_{T,WZ} > 0$. Hence $\bar{\delta}_{\rm EW} = \sigma^{\rm EW}_{\rm NLO}/\sigma^{\rm QCD}_{\rm NLO}$, which is just the ratio between the EW contribution and the QCD one.

The big panels show that the cross sections are largest in the regions where $p_{T,WZ}$ is small. The new cuts therefore reduce significantly the integrated cross sections, as shown in Table 1 and Table 2. The bottom panels show that the LL polarization has a distinctly different shape compared to the others. We see that the LL cross section falls more rapidly with increasing energy. From the middle pannels, we observe that the ratio between the EW contribution and the QCD part is different over polarizations. It is largest for the LL case, reaching 10% at around 200 GeV. The cut $p_{T,WZ} < 70$ GeV therfore does not reduce much the number of EW events. For the other polarizations, the EW part is always smaller than 5% of the QCD one, with the $W_L Z_T$ being smallest.

In Fig. 3 (W^+Z) and Fig. 4 (W^-Z) we present new results for Cut 2 and Cut 3 on the distributions of rapidity separation between the positron (or electron) and the Z boson directions. This variable is defined as

$$|\Delta y_{Z,e}| = |y_Z - y_e|, \tag{9}$$

where y_Z and y_e are the rapidities of the Z boson and of the electron/positron, respectively. These quantities can be reconstructed from the components of the particle four-momentum (see Ref. [1] for details of experimental method). The plots for Cut 1, already shown in Fig. 5 of Ref. [6], are displayed here for the sake of comparison.

Comparing Cut 1 and Cut 2, we see that the above reduction in the cross section comes from the phase space region of $|\Delta y_{Z,e}| \approx 0$, where the TT, TL, and LT are most affected, while the LL changes slightly. The TL and LT cross sections are still larger than the LL one, but the difference is small.

Moving to Cut 3, we find, very surprisingly, that the LL cross section is largest when the rapidity separation is smaller than 0.3 for the W^+Z case. The value is 0.1 for the W^-Z process. We are not surprised at this difference between the two channels because they originate from different partonic sub-processes. For the W^+Z case, the initial-state particles include $u\bar{d}$, ug, $\bar{d}g$; while they are $d\bar{u}$, $\bar{u}g$, dg for the W^-Z one. The quarks, anti-quarks, and gluons have different momentum distributions, thereby leading to the different behaviors of the polarized cross sections with respect to the $|\Delta y_{Z,e}|$ variable.

Since the LL cross section is maximal at zero separation while the TT one is maximal at around 1.2, we can further suppress the TT events by imposing an additional cut on the rapidity separation, namely $|\Delta y_{Z,e}| < \Delta y_{\rm cut}$ with $\Delta y_{\rm cut}$ in the range $[0.5, 1]$. Results for various values of $\Delta y_{\rm cut}$ are shown in Table 3. There, in the parentheses, we also provide the acceptance A, defined as the ratio of the cross section after applying the $\Delta y_{Z,e}$ cut with respect to the one before applying this cut. From the table, we observe that the LL cross section is largest when $\Delta y_{\rm cut}$ smaller than 0.6 for the W^+Z process, and 0.4 for the W^-Z case. For the combined set of events, choosing $\Delta y_{\rm cut} = 0.5$

guarantees that the LL fraction is dominant with an acceptance of 53%. We are confident that this can be done for the Run-3 data set.

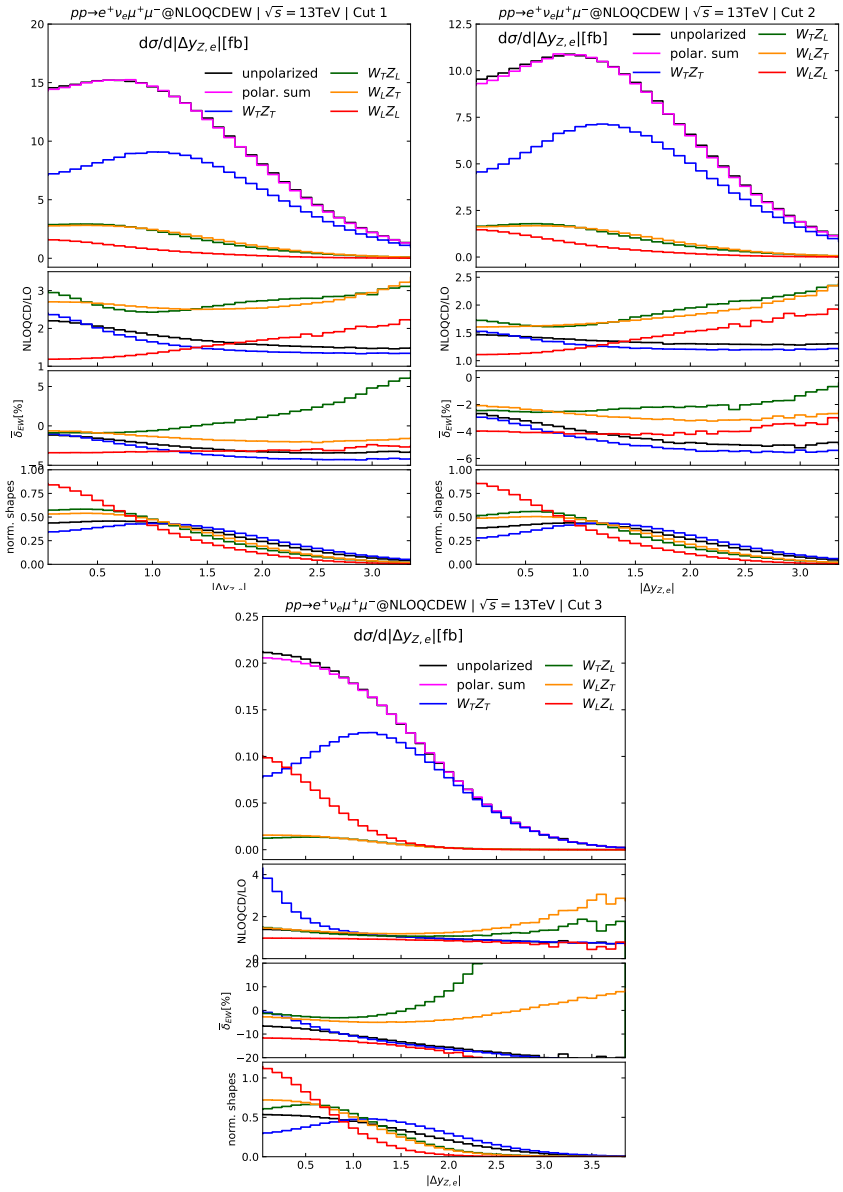

Fig. 3. Distributions in the rapidity separation (in absolute value) between the positron and the Z boson for Cut 1 (top left), Cut 2 (top right), and Cut 3 (bottom) of the W^+Z process. The big panel shows the absolute values of the cross sections at NLO QCD+EW. The middle-up panel displays the ratio of the NLO QCD cross sections to the corresponding LO ones. The middle-down panel shows $\bar{\delta}_{\rm EW}$, the EW corrections relative to the NLO QCD cross sections, in percent. In the bottom panel, the normalized shapes of the distributions are plotted.

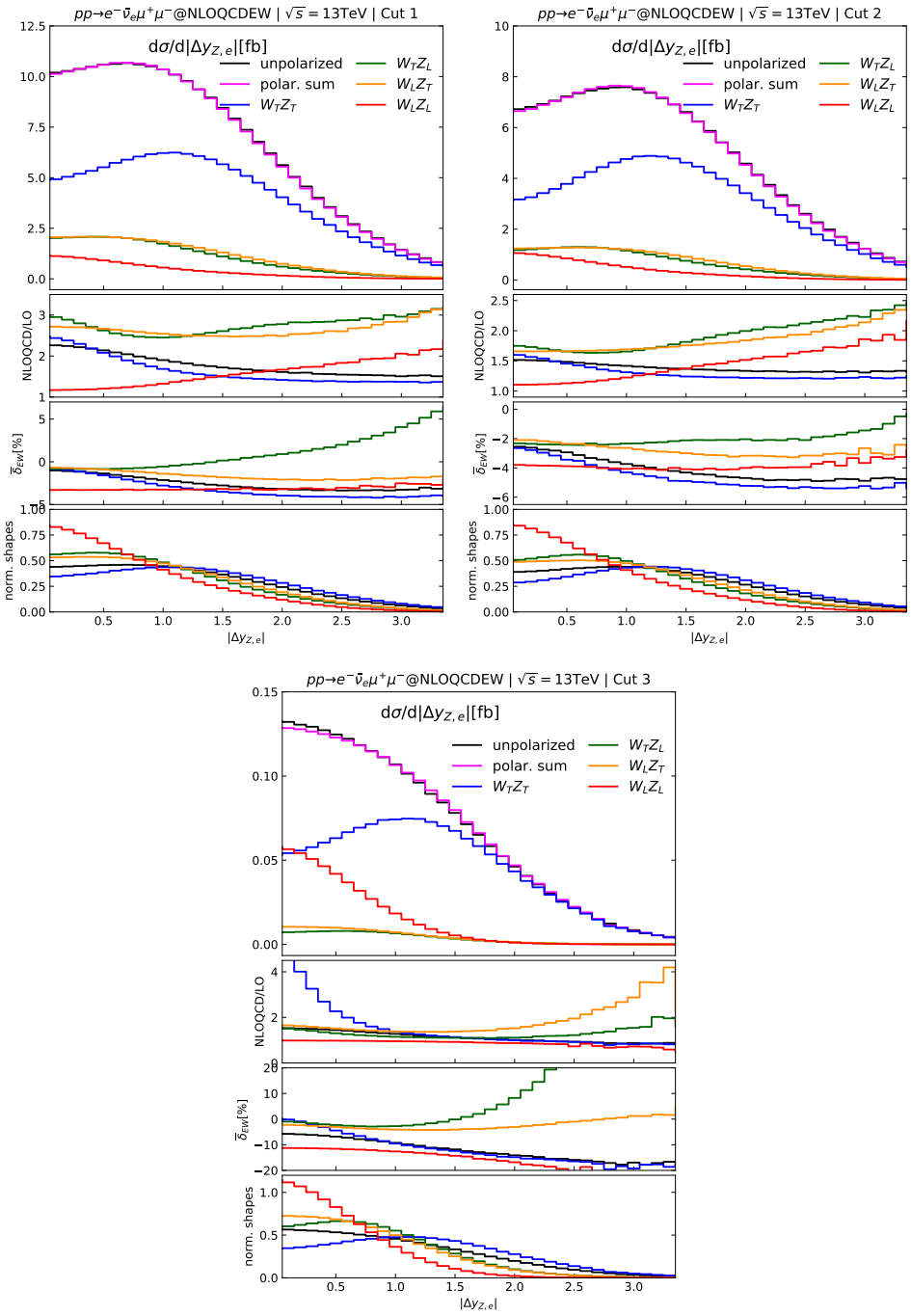

Fig. 4. Same as Fig. 3 but for the W^-Z process.

Table 3. NLO QCD+EW cross sections using the combination of Cut 3 and $|\Delta y_{Z,e}| < \Delta y_{\rm cut}$ for various values of $\Delta y_{\rm cut}$, separately for the W^+Z (left) and W^-Z (right) processes. The acceptance A, the percentage of the cross section after applying the $\Delta y_{Z,e}$ cut, is provided in the parentheses.

	W^+Z				W^-Z			
$\Delta y_{\rm cut}$	$\sigma_{\rm TT}$ [fb](A[%])	$\sigma_{\rm LL}$ [fb](A[%])	$\sigma_{\rm LT}$ [fb](A[%])	$\sigma_{\rm TL}$ [fb](A[%])	$\sigma_{\rm TT}$ [fb](A[%])	$\sigma_{\rm LL}$ [fb](A[%])	$\sigma_{\rm LT}$ [fb](A[%])	$\sigma_{\rm TL}$ [fb](A[%])
0.1	0.008(3.0)	0.010(11.4)	0.002(7.2)	0.001(6.0)	0.005(3.4)	0.006(11.4)	0.001(7.2)	0.001(6.0)
0.2	0.016(6.0)	0.020(22.6)	0.003(14.4)	0.002(12.1)	0.011(6.9)	0.011(22.6)	0.002(14.5)	0.001(12.0)
0.3	0.024(9.1)	0.029(33.3)	0.005(21.6)	0.004(18.4)	0.016(10.4)	0.017(33.3)	0.003(21.7)	0.002(18.2)
0.4	0.033(12.4)	0.038(43.3)	0.006(28.7)	0.005(24.7)	0.022(14.1)	0.022(43.3)	0.004(28.8)	0.003(24.6)
0.5	0.042(16.0)	0.046(52.5)	0.008(35.7)	0.006(31.3)	0.028(18.0)	0.027(52.5)	0.005(35.8)	0.004(31.1)
0.6	0.052(19.7)	0.053(60.7)	0.009(42.6)	0.008(37.9)	0.034(22.1)	0.031(60.8)	0.006(42.7)	0.005(37.7)
0.7	0.062(23.7)	0.060(68.0)	0.011(49.3)	0.009(44.5)	0.041(26.3)	0.034(68.0)	0.007(49.3)	0.005(44.3)
0.8	0.073(28.0)	0.065(74.2)	0.012(55.6)	0.010(51.0)	0.048(30.8)	0.038(74.3)	0.008(55.6)	0.006(50.9)
0.9	0.085(32.4)	0.070(79.5)	0.013(61.6)	0.012(57.3)	0.055(35.3)	0.040(79.7)	0.009(61.5)	0.007(57.2)
1.0	0.097(37.0)	0.074(84.0)	0.015(67.1)	0.013(63.2)	0.063(40.1)	0.043(84.1)	0.010(67.0)	0.008(63.1)

4. Conclusions

We have presented new results for doubly-polarized cross sections of the WZ production with fully leptonic decays at the LHC. Compared to the previous studies, two new kinematic cut setups are considered. These cuts are designed to observe the Radiation Amplitude Zero effect and to enhance the LL polarization. Our results show that the new cuts suppress the mixed polarizations drastically. For Cut 3, where $p_{T,WZ} < 70$ GeV and $p_{T,Z} > 200$ GeV, the dominant polarization is the TT with $f_{TT} \approx 66\%$ and the second one being the LL with $f_{LL} \approx 22\%$. We found that one can suppress the TT to make the LL dominant by imposing a new cut of $|\Delta y_{Z,e}| < 0.5$. The nice feature of this cut is that the cross sections of all polarizations are large in the selected phase-space region, therefore we still have enough number of events for the analysis.

Acknowledgment

We thank our experimental colleagues, in particular Joany Manjarrés and Junjie Zhu, for useful discussions. This research is funded by the Vietnam National Foundation for Science and Technology Development (NAFOSTED) under grant number 103.01-2020.17.

References

[1] ATLAS Collaboration, *Observation of gauge boson joint-polarisation states in $W^{\pm}Z$ production from pp collisions at $\sqrt{s} = 13$ TeV with the ATLAS detector*, Phys. Lett. B **843** (2023) 137895

[2] J. A. Aguilar-Saavedra and J. Bernabeu, *Breaking down the entire W boson spin observables from its decay*, Phys. Rev. D **93** (2016) 011301
[3] A. Denner and G. Pelliccioli, *Polarized electroweak bosons in W^+W^- production at the LHC including NLO QCD effects*, J. High Energy Phys. **09** (2020) 164.
[4] A. Denner and G. Pelliccioli, *NLO QCD predictions for doubly-polarized WZ production at the LHC*, Phys. Lett. B **814** (2021) 136107
[5] D. N. Le and J. Baglio, *Doubly-polarized WZ hadronic cross sections at NLO QCD + EW accuracy*, Eur. Phys. J. C **82** (2022) 917
[6] D. N. Le, J. Baglio and T. N. Dao, *Doubly-polarized WZ hadronic production at NLO QCD+EW: calculation method and further results*, Eur. Phys. J. C **82** (2022) 1103
[7] A. Denner, C. Haitz and G. Pelliccioli, *NLO QCD corrections to polarised di-boson production in semi-leptonic final states*, Phys. Rev. D **107** (2023) 053004.
[8] A. Denner and G. Pelliccioli, *NLO EW and QCD corrections to polarized ZZ production in the four-charged-lepton channel at the LHC*, J. High Energy Phys. **2021** (2021) 97.
[9] R. Poncelet and A. Popescu, *NNLO QCD study of polarised W^+W^- production at the LHC*, J. High Energy Phys. **07** (2021) 023.
[10] ATLAS Collaboration, *Measurement of the $W^\pm Z$ boson pair-production cross section in pp collisions at $\sqrt{s} = 13$ TeV with the ATLAS Detector*, Phys. Lett. B **762** (2016) 1.
[11] ATLAS Collaboration, *Measurement of $W^\pm Z$ production cross sections and gauge boson polarisation in pp collisions at $\sqrt{s} = 13$ TeV with the ATLAS detector*, Eur. Phys. J. C **79** (2019) 535.
[12] R. Franceschini, G. Panico, A. Pomarol, F. Riva and A. Wulzer, *Electroweak Precision Tests in High-Energy Diboson Processes*, J. High Energy Phys. **02** (2018) 111.
[13] U. Baur, T. Han and J. Ohnemus, *Amplitude zeros in W+- Z production*, Phys. Rev. Lett. **72** (1994) 3941.
[14] A. Denner, S. Dittmaier, M. Roth and D. Wackeroth, *Electroweak radiative corrections to $e^+e^- \to WW \to 4$ fermions in double pole approximation: The RACOONWW approach*, Nucl. Phys. B **587** (2000) 67.
[15] G. Watt and R. S. Thorne, *Study of Monte Carlo approach to experimental uncertainty propagation with MSTW 2008 PDFs*, J. High Energy Phys. **08** (2012) 052.
[16] J. Gao and P. Nadolsky, *A meta-analysis of parton distribution functions*, J. High Energy Phys. **07** (2014) 035.
[17] L. A. Harland-Lang, A. D. Martin, P. Motylinski and R. S. Thorne, *Parton distributions in the LHC era: MMHT 2014 PDFs*, Eur. Phys. J. C **75** (2015) 204.
[18] NNPDF Collaboration, *Parton distributions for the LHC Run II*, J. High Energy Phys. **04** (2015) 040.
[19] J. Butterworth, S. Carrazza, A. Cooper-Sarkar, A. De Roeck, J. Feltesse, S. Forte et al., *PDF4LHC recommendations for LHC Run II*, J. Phys. G **43** (2016) 023001.
[20] S. Dulat, T.-J. Hou, J. Gao, M. Guzzi, J. Huston, P. Nadolsky et al., *New parton distribution functions from a global analysis of quantum chromodynamics*, Phys. Rev. D **93** (2016) 033006.
[21] D. de Florian, G. F. R. Sborlini and G. Rodrigo, *QED corrections to the Altarelli-Parisi splitting functions*, Eur. Phys. J. C **76** (2016) 282.
[22] S. Carrazza, S. Forte, Z. Kassabov, J. I. Latorre and J. Rojo, *An Unbiased Hessian Representation for Monte Carlo PDFs*, Eur. Phys. J. C **75** (2015) 369.
[23] A. Manohar, P. Nason, G. P. Salam and G. Zanderighi, *How bright is the proton? A precise determination of the photon parton distribution function*, Phys. Rev. Lett. **117** (2016) 242002.
[24] A. V. Manohar, P. Nason, G. P. Salam and G. Zanderighi, *The photon content of the proton*, J. High Energy Phys. **12** (2017) 046.
[25] A. Buckley, J. Ferrando, S. Lloyd, K. Nordström, B. Page, M. Rüfenacht et al., *LHAPDF6: parton density access in the LHC precision era*, Eur. Phys. J. C **75** (2015) 132.